Quasi-Spherical Focal Spot in Two-Photon Scanning Microscopy by Three-Ring Apodization

CRISTINA IBÁÑEZ-LÓPEZ,[1] GENARO SAAVEDRA,[1] KARSTEN PLAMANN,[1] GILBERT BOYER,[1] AND MANUEL MARTÍNEZ-CORRAL[2]*
[1]*Applied Optics Laboratory, ENSTA-Ecole Polytechnique, 91761 Palaiseau, France*
[2]*Department of Optics, Universitat de València, E46100 Burjassot, Spain*

KEY WORDS two-photon excitation; optical sectioning effect; beam shaping

ABSTRACT We present a beam-shaping technique for two-photon excitation (TPE) fluorescence microscopy. We show that by inserting a properly designed three-ring pupil filter in the illumination beam of the microscope, the effective optical sectioning capacity of such a system improves so that the point spread function gets a quasi-spherical shape. Such an improvement, which allows the acquisition of 3D images with isotropic quality, is obtained at the expense of only a small increase of the overall energy in the axial sidelobes. The performance of this technique is illustrated with a scanning TPE microscopy experiment in which the image of small beads is obtained. We demonstrate an effective narrowing of 12.5% in the axial extent of the point spread function, while keeping the 82% of the spot-fluorescence efficiency. *Microsc. Res. Tech. 67:22–26, 2005.*

INTRODUCTION

The noninvasive imaging of three-dimensional (3D) samples is often required in many branches of science, from solid-state physics to biomedical inspection. In this case, a depth-sectioning technique is mostly used. Conventional wide-field optical microscopes provide very poor sectioning power, since an image focused at a certain depth in the specimen contains blurred information from the entire one. This fact gives rise to 3D images with strongly deteriorated contrast. Several techniques have been developed to avoid this drawback. In particular, the use of single-photon fluorescence confocal scanning microscopes (Pawley, 1995) is widely spread. In this technique, a pinholed detection provides an uncommon depth discrimination capacity. However, the practical implementation of the setup leads to some difficulties. On the one hand, since the entire sample is illuminated when any single plane is imaged, photobleaching is an important effect after the whole scanning of large samples. On the other hand, the pinholed detection imposes high sensitivity to misalignment and poor signal-to-noise ratio in detection.

To overcome these drawbacks, the alternative use of multiphoton scanning microscopy has been proposed. This technique is based on the simultaneous absorption of two or more photons by the fluorophores, following which a single fluorescence photon is emitted. Special attention has been paid to two-photon excitation (TPE) scanning microscopes (Denk et al., 1990), in which two photons with nearly equal wavelengths are absorbed by the sample (Göppert-Mayer, 1931). The excitation wavelength is typically twice bigger than in the single-photon case. Since the fluorescence intensity is proportional to the square of the illumination intensity, TPE microscopes have the ability of strongly limiting the excitation region, providing both reduction of photobleaching and inherent optical sectioning capacity despite the absence of pinholed detection.

The resolving power of a microscope is usually evaluated in terms of its point spread function (PSF), which in the TPE case is defined as the fluorescence emission distribution generated by a light point source. The fluorescence emission is proportional to the probability of simultaneous absorption of two low-energy photons. Since two statistically independent events have to occur, this probability is proportional to the square of the excitation intensity. The PSF of TPE microscopes, as in the single-photon case, is governed by diffraction and therefore is much wider in the axial direction than in the lateral one. This implies that, in spite of their proverbial depth discrimination capacity, the axial resolution of TPE microscopes is much poorer than their lateral resolution. This fact leads to anisotropic 3D imaging quality.

The search for the solution of these troubles has focused the attention of some researchers recently. We can cite the confocal theta microscope (Stelzer and Lindek, 1994), in which the illumination and detection axis are set orthogonal to each other, providing an effective reduction in the 3D imaging anisotropy. A similar approach has been recently reported in the so-called selective plane illumination microscopy (Huisken et al., 2004). In 4Pi-confocal microscopes (Blanca et al., 2001), two opposing, high-NA objectives

*Correspondence to: Manuel Martínez-Corral, Departamento de Óptica, Universitat de València, E46100 Burjassot, Spain. E-mail: manuel.martinez@uv.es

Received 19 November 2004; accepted in revised form 10 March 2005

C. Ibáñez-López's present address is Department of Optics, Universitat de València, E46100 Burjassot, Spain.
Genaro Saavedra's present address is Department of Optics, Universitat de València, E46100 Burjassot, Spain.

Contract grant sponsor: Plan Nacional I+D+I (Ministerio de Ciencia y Tecnología, Spain); Contract grant number: grant DPI2003-4698; Contract grant sponsor: Ministerio de Ciencia y Tecnología, Spain; Contract grant number: HF2003-0257.
DOI 10.1002/jemt.20175
Published online in Wiley InterScience (www.interscience.wiley.com).

are used to coherently illuminate the fluorescent sample and, therefore, to create an axially-narrowed interferencial focal spot. The stimulated emission depletion microscopy (Klar et al., 2001) uses the inhibition of fluorophores at the outer region of the scanning excitation spot to break the diffraction barrier of this stretching. Finally, an alternative type of TPE process, which uses two photons with different wavelengths, known as two-color excitation fluorescence, has been extensively demonstrated in the past few years (Lakowicz et al., 1996; Gryczynski et al., 1997), and applied to different optical sectioning architectures (Lindek and Stelzer, 1999; Lim and Saloma, 2002; Xiao et al., 2003). In this case, the PSF of the microscope is proportional to the product of two differently-scaled excitation intensities, and is generated only in regions where the excitation beams overlap each other in space and time.

An alternative technique to reduce the PSF anisotropy is based on the use of pupil filters. In past years, the use of purely absorbing or complex-transmittance pupil masks has been proposed to improve the axial resolution of single-photon confocal microscopes (Hegedus and Sarafis, 1986; Ding et al., 1997; Kowalczyk et al., 1998; Sheppard, 1999; Neil et al., 2000; Martínez-Corral et al., 2002; Boyer, 2002; Boyer, 2003; Martínez-Corral et al., 2003a) and multiphoton architectures (Blanca and Hell, 2002; Martínez-Corral et al., 2003b; Ibáñez-López et al., 2004; Chon and Gu, 2004). Different from other proposals, these techniques, also known as PSF engineering, pose a minimum modification of microscopes architecture, although they provide a significant improvement of their performance.

The aim of this work is to improve the optical-sectioning capacity of TPE microscopes by insertion of simple, easy-to-manufacture, beam-shaping elements. Specifically, we propose and experimentally verify the use of annular binary filters composed of three transparent rings. These filters have the ability of compressing the central lobe of the axial PSF but keeping under control the increase of height of the axial side lobes inherent usually to any superresolving beam-shaping element. We have performed the experimental measurement of the PSF provided by the optimum three-annular filter, and found a 12.5% compression of the PSF along the axial direction. Besides, this compression does not produce any significant enlargement of the axial side lobes. Therefore, we can state that the insertion of such three-annular filters in a TPE scanning microscope can lead to an effective, significant improvement of its optical sectioning capacity.

MATERIALS AND METHODS

Let us consider the irradiance PSF, h_{2p}, of a TPE fluorescence scanning microscope, sketched in Figure 1. As stated above, this function is proportional to the square of the illumination irradiance distribution, i.e.,

$$h_{2p}(r,z;\lambda) = h_{ill}^2(r,z;\lambda), \tag{1}$$

where the illumination PSF $h_{ill}(r,z;\lambda)$ is given, according to the scalar Debye approximation (Gu, 2000), by

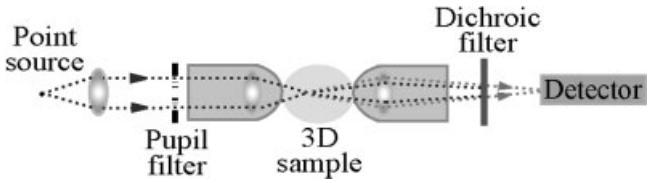

Fig. 1. Schematic geometry of the TPE scanning microscope.

$$h_{ill}(r,z;\lambda) = \left| \int_0^1 t(\rho) \mathrm{J}_0\left(\frac{2\pi}{\lambda} r\rho \sin\alpha\right) \exp\left\{-i2\pi z \frac{\sqrt{1-\rho^2\sin^2\alpha}}{\lambda}\right\} \frac{\sin^2\alpha}{\sqrt{1-\rho^2\sin^2\alpha}} \rho\, d\rho \right|^2. \tag{2}$$

In this equation, α is the aperture angle of the objective lens, and $t(\rho)$ accounts for the amplitude transmittance of the illumination objective-lens aperture stop. Besides, r and z are the cylindrical coordinates as measured from the focal point, whereas ρ is the normalized radial coordinate at the aperture stop. The wavelength of the illuminating beam inside the sample is denoted by λ. Note that, as pointed out by Juškaitis (2003), this scalar approximation works remarkably well up to angular apertures of about $\alpha = 60^\circ$. More accurate calculations should be based on the vectorial Debye theory (Richards and Wolf, 1959).

Since the aim of this work is the improvement of axial resolution, we fix our attention in the axial behavior of the PSF in Eq. (1). Following the same procedure as Ibáñez-López et al. (2004), we set $r = 0$ and perform the nonlinear mapping

$$\zeta = \frac{\sqrt{1-\rho^2\sin^2\alpha} - \cos\alpha}{\cos\alpha - 1} + 0.5; \quad q(\zeta) = t(\rho), \tag{3}$$

to straightforwardly obtain

$$h_{2p}(0,z_N;\lambda) = \left| (1-\cos\alpha) \int_{-0.5}^{+0.5} q(\zeta) \exp(-i2\pi z_N \zeta) d\zeta \right|^4. \tag{4}$$

Where z_N is the normalized axial coordinate defined as

$$z_N = \frac{2\sin^2(\alpha/2)}{\lambda} z. \tag{5}$$

Equation (5) shows that the axial behaviour of the PSF of the system is fully governed by the 1D Fourier transform of the mapped pupil $q(\zeta)$. In this way, the design of beam-shaping elements to tailor the axial PSF of a TPE microscope will be simply supported on the properties of this transformation. Our approach for the selection process is based on the concept of axial gain in resolution, which is defined here as the

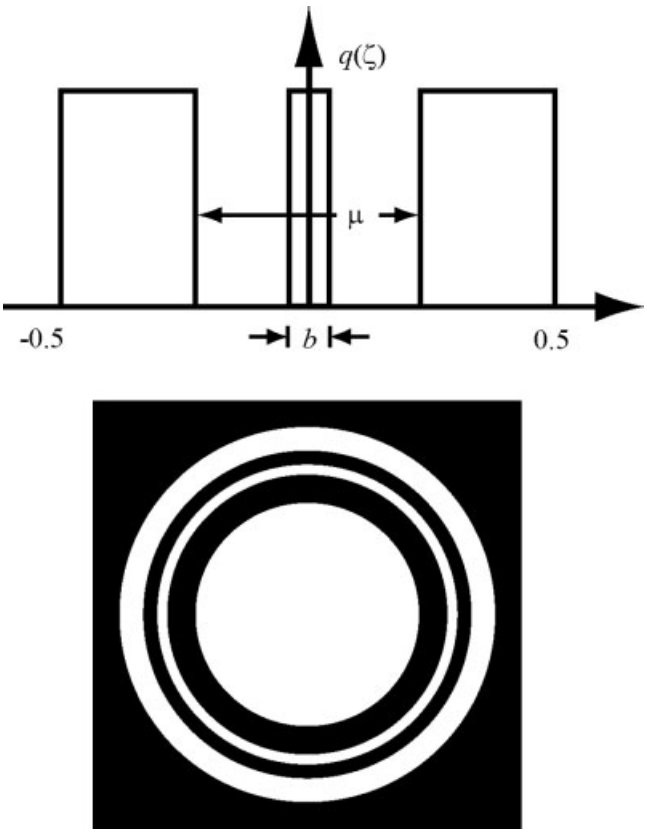

Fig. 2. Mapped transmittance of a 3R filter (**top**) and actual 2D representation (**bottom**).

quotient between the width of the main peak of the axial PSF of the TPE microscope in which the selected filter is inserted, and the one corresponding to the reference non-apodized TPE scanning microscope. Following an approach equivalent to that reported by Martínez-Corral et al. (1999), and after straightforward calculations, it is found that the axial gain is given by

$$G_A = \frac{\sigma_a}{\sigma_c}, \tag{6}$$

σ_a and σ_c being the standard deviation of the mapped pupil $q(\zeta)$ for the apodized and non-apodized cases, respectively. Note that this value for the gain is identical to the axial gain corresponding to the illumination subsystem of the microscope itself in a one-photon excitation setup.

To effectively improve the TPE axial resolution, we propose to insert in the illuminating beam a filter with the ability to compress the main peak of its corresponding axial spot (i.e., providing $G_A > 1$), but controlling the inherent reinforcement of sidelobes energy. Adapting Boyer's concept (Boyer, 1983) to the axial PSF, we propose the use of the family of binary masks known as three-ring (3R) filters (Martínez-Corral et al., 2003a). These filters are composed of two transparent rings surrounding a clear aperture. A representation in terms of the functions $t(\rho)$ and $q(\zeta)$ for a typical 3R filter is presented in Figure 2. Each member of the family

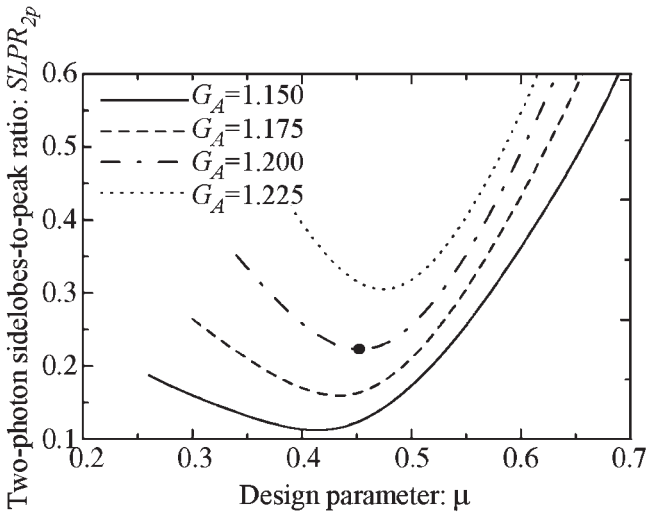

Fig. 3. *SLPR* values for families of filters with the same axial gain G_A.

is uniquely defined by the construction parameters b and $1 - \mu$. These parameters are directly related to the light throughput of the intermediate annulus and of the rest of the filter, respectively. It is easy to obtain that for these filters the axial gain is given by

$$G_A = \sqrt{\frac{1 - \mu^3 + b^3}{1 - \mu + b}}. \tag{7}$$

Note that all pairs (b,μ) fulfilling Eq. (7) for a given G_A correspond to 3R filters with the same axial gain. Thus, for a selected axial stretching, we can choose the 3R filter that minimizes the redistributed sidelobe energy. As a measure of the focused light efficiency in the TPE configuration, we use the two-photon sidelobes-to-peak ratio ($SLPR_{2p}$), defined as

$$SLPR_{2p} = \frac{\int_{z_0}^{+\infty} h_{2p}(0,z;\lambda)dz}{\int_0^{z_0} h_{2p}(0,z;\lambda)dz} = \frac{\int_{z_0}^{+\infty} h_{ill}^2(0,z;\lambda)dz}{\int_0^{z_0} h_{ill}^2(0,z;\lambda)dz}, \tag{8}$$

where z_0 corresponds to the z-coordinate of the first zero-intensity axial point. In Figure 3, we draw several curves with constant G_A but varying $SLPR_{2p}$. Any point of the curve corresponds to a different (b,μ) pair. Note that, since for a given axial gain not all pairs (b,μ) correspond to a physically realizable filter, each curve in Figure 3 has been represented in a different interval of μ. The minimum in each curve of constant G_A, gives the parameter μ that corresponds to the filter with minimum sidelobe energy. The solution of Eq. (7) provides the value of b that completes the characterization of the optimum filter.

Although theoretically it is possible to choose any a priori value for the axial gain, practical restrictions appear if the light efficiency of the system is taken into account. In Figure 4, we represent the value of the TPE light throughput of the optimum filter as a function of its axial gain. It is direct to conclude that the

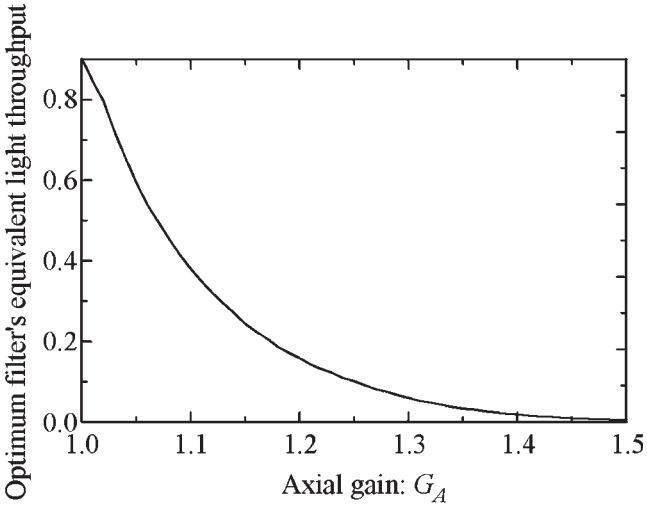

Fig. 4. TPE light efficiency for the optimum filter as a function of the gain it provides.

greater the demanded gain, the lower the light efficiency of the filter. For this reason, some kind of trade-off is needed in practice.

RESULTS AND DISCUSSION

We present next an experimental verification of the proposed technique. We test the performance of our optimum filter by measuring its PSF in a TPE microscope. We used a mode-locked Cr^{4+}:Forsterite laser to provide the illumination for the experience. This source produced pulses with central wavelength $\lambda = 1{,}260$ nm and mean temporal width $\Delta t = 50$ fs at a repetition rate of 84 MHz. The mean power obtained over the sample was around 200 mW. For the illumination and collection, we used two identical infinity-corrected objectives from Olympus (UPlan APO/IR 1.2 W 60×). The selected 3R filter was inserted in the entrance pupil plane of the illumination objective. The external diameter of the filter was adjusted to fit the effective size of the clear pupil of the objective itself. For the implementation of the filter, we used a high-contrast photographic film (Kodak Technical Pan). The sample consisted of fluorescent spheres (beads) of 200 nm in diameter stuck between two coverslips. Since the size of these beads was much smaller than the PSF of the microscope for the illuminating wavelength, a measure of the image of these test objects provided a good approximation to the actual PSF of the setup. A scheme of the experimental setup is presented in Figure 5. The synchronous detection through the chopper and the lock-in amplifier were used to increase the signal-to-noise ratio of the low detection signal.

The selection of the specific 3R filter for the experiment was made balancing the axial gain and the light efficiency of the system. We chose a filter with parameters $\mu = 0.45$ and $b = 0.081$, which minimized the $SLPR_{2p}$ for an axial gain $G_A = 1.20$ (see curve in Fig. 4). In fact, this filter is the one represented in Figure 2. In this optimum case, the theoretical $SLPR_{2p}$ was 0.224, while in the nonapodized case it is 0.0029. In terms of light-spot efficiency, calculated as $100/(1 +$

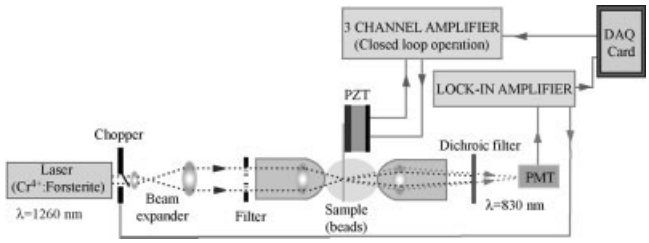

Fig. 5. Diagram of the experimental TPE scanning microscopy setup.

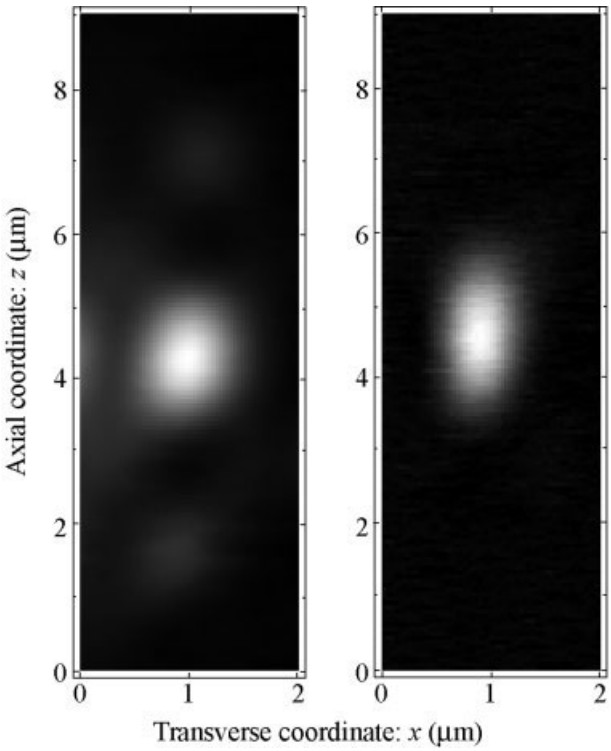

Fig. 6. 2D gray-scale sections of the experimental 3D PSFs obtained in the 3R apodized TPE experiment (**left**) and the nonapodized TPE setup (**right**).

$SLPR_{2p}$), this filter maintains an acceptable value of 82% in front of the 99% in the nonapodized TPE setup. In Figure 6, we present typical results for the experimental PSFs obtained with and without the filter. To obtain theses figures, the bead was scanned through a meridian plane containing the optical axis of the objective. Note that the PSF obtained with the 3R filter is clearly stretched along the axial direction. In Figure 7, we have plotted an axial profile of the above PSFs. The numerical evaluation of the axial *FWHM* gives values of 1.26 μm for our optimum apodization versus 1.44 μm for the clear aperture TPE. It follows, thus, a significant narrowing of 12.5% in the axial PSF. Numerical evaluation of this PSF predicted a theoretical stretching of 14.7%, in acceptably good agreement with the experimental result. Note also from Figure 6 that, since no significant dilation in the transverse direction is observed on the apodized result, a symmetrization of the 3D PSF is effectively achieved. This quasi-spherical

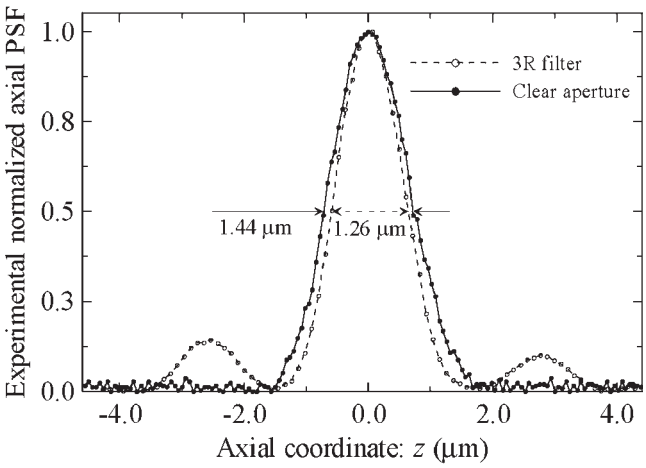

Fig. 7. Axial profile of the experimental PSFs in Figure 6.

response leads to a clear improvement of the isotropy of the imaging features of the microscope.

CONCLUSIONS

We have proven that the use of a special class of beam-shaping elements permits substantial improvement of the optical sectioning capacity of the TPE scanning microscopes. Specifically, we have verified in a typical TPE experiment that the 3R filters allows stretching the main-peak of the axial PSF. This stretching does produce, collaterally, neither a substantial enlargement of the axial sidelobes nor a relevant widening of the PSF in the transverse direction. So, we have obtained a quasi-spherical PSF, which can allow the acquisition of high-resolution 3D images with isotropic quality. Note finally that although our approach and design procedure has been made on the basis of the scalar diffraction theory, the experimental results show an acceptably good agreement with the calculations. This is because the 3R filters are immune to the depolarization effect (Martínez-Corral et al., 2004).

ACKNOWLEDGMENTS

This work has been mainly funded by the Plan Nacional I+D+I (grant DPI2003-4698), Ministerio de Ciencia y Tecnología, Spain. C. Ibáñez-López gratefully acknowledges financial support from the same institution. The stay of G. Saavedra in the LOA was funded by the Acción Integrada HF2003-0257, Ministerio de Ciencia y Tecnología, Spain.

REFERENCES

Blanca CM, Hell SW. 2002. Axial superresolution with ultrahigh aperture lenses. Opt Express 10:893–898.

Blanca CM, Bewersdorf J, Hell SW. 2001. Single sharp spot in fluorescence microscopy of two opposing lenses. Appl Phys Lett 79:2321–2323.

Boyer G. 1983. Réalisation d'un filtrage super-résolvant. Opt Acta 30:807–816.

Boyer G. 2002. New class of axially apodizing filters for confocal scanning microscopy. J Opt Soc Am A 19:584–589.

Boyer G. 2003. 3D Behaviour of Frieden filters in confocal imaging. Micron 37:275–282.

Chon JW, Gu M. 2004. Scanning total internal reflection fluorescence microscopy under one-photon and two-photon excitation: image formation. Appl Opt 43:1063–1071.

Denk W, Strickler JH, Webb WW. 1990. Two-photon laser scanning fluorescence microscopy. Science 248:73–76.

Ding Z, Wang G, Gu M, Wang Z, Fan Z. 1997. Superresolution with an apodization film in a confocal setup. Appl Opt 36:360–363.

Göppert-Mayer M. 1931. Über Elementarakte mit zwie Quantensprüngen. Ann Phys (Leipzig) 9:273–294.

Gryczynski I, Malak H, Lakowitz R. 1997. Two-color two-photon excitation of indole. Biospect 3:97–101.

Gu M. 2000. Advanced optical imaging theory. Berlin: Springer-Verlag.

Hegedus ZS, Sarafis V. 1986. Superresolving filters in confocally scanned imaging systems. J Opt Soc Am A 3:1892–1896.

Huisken J, Swoger J, Del Bene F, Wittbrodt J, Stelzer EHK. 2004. Optical sectioning deep inside live embryos by selective plane illumination microscopy. Science 305:1007–1009.

Ibáñez-López C, Escobar I, Saavedra G, Martínez-Corral M. 2004. Optical-sectioning improvement in two-color excitation scanning microscopy. Microsc Res Tech 64:96–102.

Juškaitis R. 2003. Characterizing high numerical aperture microscope objective lenses. In: Optical imaging and microscopy. Török P, Kao FG, editors. Opt Imag Microsc. Berlin: Springer.

Klar TA, Engel E, Hell SW. 2001. Breaking Abbe's diffraction resolution limit in fluorescence microscopy with stimulated emission depletion beams of various shapes. Phys Rev E 64:1–9.

Kowalczyk M, Zapata-Rodríguez CJ, Martínez-Corral M. 1998. Asymmetric Apodization in Confocal Scanning Systems. Appl Opt 37: 8206–8214.

Lakowicz JR, Gryczynski I, Malak H, Gryczynski Z. 1996. Two-color two-photon excitation fluorescence. Photochem Photobiol 64: 632.

Lim M, Saloma C. 2002. Confocality condition in two-color excitation microscopy with two focused excitation beams. Opt Commun 207: 121–130.

Lindek S, Stelzer EHK. 1999. Resolution improvement by nonconfocal theta microscopy. Opt Lett 24:1505–1507.

Martínez-Corral M, Andrés P, Zapata-Rodríguez CJ, Kowalczyk M. 1999. Three-dimensional superresolution by annular binary filters. Opt Commun 165:267–278.

Martínez-Corral M, Caballero MT, Stelzer EHK, Swoger J. 2002. Tailoring the axial shape of the point spread function using the Toraldo concept. Opt Express 10:98–103.

Martínez-Corral M, Ibáñez-López C, Caballero MT, Muñoz-Escrivá L, Saavedra G. 2003a. Three-ring filters increase the effective NA up to 1.46 in optical sectioning fluorescence microscopy. J Phys D 36: 1669–1674.

Martínez-Corral M, Ibáñez-López C, Saavedra G, Caballero MT. 2003b. Axial gain in resolution in optical sectioning fluorescence microscopy by shaded-ring filters. Opt Express 11:1740–1745.

Martínez-Corral M, Martínez-Cuenca R, Escobar I, Saavedra G. 2004. Reduction of focus size in tightly focused linearly polarized beams. Appl Phys Lett 85:4319–4321.

Neil MAA, Juškaitis R, Wilson T, Laczik ZJ, Sarafis V. 2000. Optimized pupil-plane filters for confocal microscope point-spread function engineering. Opt Lett 25:245–247.

Pawley JB. 1995. Handbook of biological confocal microscopy. New York: Plenum Press.

Richards B, Wolf E. 1959. Electromagnetic diffraction in optical systems. II. Structure of the image field in an aplanatic system. Proc R Soc (Lond) A 253:358–379.

Sheppard CJR. 1999. Binary optics and confocal imaging. Opt Lett 24:505–506.

Stelzer EHK, Lindek S. 1994. Fundamental reduction of the observation volume in far-field light microscopy by detection orthogonal to the illumination axis: confocal theta microscopy. Opt Commun 111: 536–547.

Xiao F, Wang G, Xu Z. 2003. Superresolution in two-color excitation fluorescence microscopy. Opt Commun 228:225–230.